A VSM-Based DER Dispatch MINLP for Volt-VAR Control in Unbalanced Power Distribution Systems

Catie McEntee, David Mulcahy, Jiyu Wang, Xiangqi Zhu, Ning Lu
Electrical and Computer Engineering Department
North Carolina State University
Raleigh, NC, USA
cmmcente@ncsu.edu

***Abstract*—This paper presents an optimal dispatch algorithm to coordinate customer-owned controllable loads and smart solar inverters with utility-owned voltage regulators and capacitors to meet voltage control objectives. The optimization problem is formulated as a mixed-integer nonlinear programming (MINLP) problem. A voltage sensitivity matrix (VSM) is used to linearize the effect of control actions on the voltage at customer nodes when solving the MINLP. The VSM is recalculated at each time step to improve the computational accuracy. Both discrete switching actions of the capacitor and VRs and the continuous adjustment of real and reactive power from load and smart inverters are considered in the MINLP volt-var problem formulation. The objective function minimizes the cost of all control actions and the magnitude of voltage fluctuations from the previous time period. Constraints ensure that the voltage at each node is maintained within ANSI limits and the feeder power factor is controlled within the desired range. The algorithm is tested using an actual 3-phase unbalanced distribution feeder model. Simulation results demonstrate that the proposed algorithm is computationally feasible on real circuits and improves voltage control while minimizing operational costs.**

***Index Terms*—Demand-Side Management, Mixed-Integer Nonlinear Programming, Power Distribution, Reactive Power Control, Voltage Control**

I. INTRODUCTION

High penetration of solar generation on distribution circuits can cause violations of voltage standards, larger voltage fluctuations, and increased utility-owned device operations [1]. In high solar penetration circuits, voltage control is increasingly difficult if relying solely on traditional voltage control devices like capacitors, on-load tap changers (LTC) and line voltage regulators (VRs). Thus, it is increasingly important to develop advanced voltage control methods that coordinate all available resources to manage voltage in real-time.

While the integration of photovoltaics (PV) can worsen these voltage issues, PV inverters can provide reactive power for cheaper and more continuous voltage control than conventional resources. Combined with the smart controls for customer loads, these customer-owned distributed energy resources (DERs) can control voltages on feeders more precisely with smaller voltage fluctuations [2]. Conventional voltage control schemes utilize capacitors and VRs designed to meet control objectives during forecasted peaks only. As a result, capacitors and VRs have fixed local set points that are not adapted frequently in response to a wider range of system operation conditions (e.g., low and high loads, high and low PV production). In addition, control actions of VRs and capacitors are discrete (i.e., changing regulator taps and switching capacitors in/out), causing a large voltage fluctuation during each switching event. The mechanical switches and tap changers also accumulate wear-and-tear each time they operate.

Installing VR devices requires substantial capital investments, yet they are relatively inflexible and ill-suited to regulate fast changing voltages caused by high-penetration of variable solar generation resources. Therefore, there has been growing interest and research in developing DER-based volt-var control algorithms which utilize smart inverters and controllable loads in coordination with the utility-owned assets to regulate voltage variations [1]-[7]. Several papers have used voltage sensitivity matrices (VSM) based on simulation results [2] or linearized power flow equations [3]-[5], [8] to effectively estimate the effect of control actions taken by utility- and consumer-owned resources. Coupled with optimization programs, VSMs have been shown to successfully control voltage using these assets [2], [6], [7]. Several of these have proven effective on circuits with high penetrations of PV [1], [2], [9], [10]. These methods have the advantage of being capable of controlling voltage in a more active manner in response to a wider range of operating conditions. However, the current research has been limited to small IEEE test systems [4], [7], [10], systems with balanced phases [1], [7], [9], [10], and cases that use only a subset of the consumer- or utility-owned resources [2], [6], [10]. To fully utilize distribution resources, volt-var strategies need to schedule and operate multiple resource types concurrently and optimally. Thus, each resource needs to be weighted by its capability to regulate voltage variations and the cost of operation. Additionally, the method needs to be scalable so that optimal dispatch commands can be generated for distribution feeders consisting of hundreds of load nodes and smart inverter units in real-time.

Funded by the U.S. Department of Energy SunShot Initiative

Thus, in this paper, we present a volt-var algorithm that optimizes the dispatch of customer resources including load and PV systems' real and reactive power along with VRs and capacitors. The optimization problem is formulated as a mixed-integer nonlinear programming (MINLP) problem. A voltage sensitivity matrix (VSM) is used to linearize the effect of control actions on the voltage at customer nodes when solving the MINLP. The VSM is recalculated at each time step to reflect the latest operating condition, an improvement on the averaged VSM used in [2]. Both discrete switching actions of the capacitor and VRs and the continuous adjustment of real and reactive power from load and smart inverters are considered in the MINLP volt-var problem formulation. The objective function minimizes the cost of all control actions and the magnitude of voltage fluctuations from the previous time period. Constraints ensure that the voltage at each node is maintained within ANSI limits and the feeder power factor is controlled within the desired range.

The algorithm is tested on a 3-phase unbalanced distribution feeder model representing a real circuit in rural North Carolina. The feeder includes 998 buses, 371 of which are load buses. Simulation results demonstrate that our algorithm is effective, accurate, and computationally feasible for real-time applications.

II. MINLP-BASED VOLT-VAR CONTROL ALGORITHM

We assume that a centralized DER and utility resource controller at the distribution control center will execute the volt-var control algorithm every 5 minutes. Customer-owned resources include controllable loads and PV systems with smart inverters. Utility-based resources include switched capacitors and LTC/VRs.

At the core of the volt-var control algorithm is the VSM-based linearized voltage calculation and the MINLP-based optimal dispatch. The MINLP determines the optimal schedule for each resource's operation for each time step by minimizing the cost of dispatch and the voltage change between time steps. The MINLP's constraints maintain voltage and power factor within the desired limits and customer- and utility-owned resources within their operating limits. The VSM approximates the voltage response across the circuit due to operation of the controllable resources so that we don't need to solve power flows for each MINLP iteration.

A. Voltage Sensitivity Matrix

The proposed VSM method accounts for current operating conditions by calculating a new set of sensitivity factors at the beginning of each 5-minute control interval. Note that we define L as the set of all controllable load nodes, K as the set of all PV nodes, $N = L \cup K$ as the set of all load and/or PV nodes, M as the set of all capacitor banks, and R as the set of all VRs, including the LTC at the feeder head. First, a power flow is run with current loads, PV outputs, capacitor status, and VR tap settings to calculate the voltages V_i^{Base} at each node i in N. Then, the real power injected at each node, j, in N is perturbed by a small value, ΔP, one node at a time, and the resulting voltages, $V_{i,j}^P$, for each node, i, in N are recorded. The sensitivity factors with respect to real power injection are calculated using (1). Similarly, the voltage sensitivity to reactive power is calculated by perturbing the reactive power injected at each node, j, in N by a small value, ΔQ, and recording the resulting voltages, $V_{i,j}^Q$, for use in equation (2). To find the sensitivity to capacitor switching, the status of each capacitor, m, in M is toggled from its current position, one at a time, and the resulting voltages, $V_{i,m}^{cap}$, for each node, i, in N are recorded and used in equation (3). Finally, the sensitivity to tap changes is calculated by adjusting the position of each VR, r, in R up one tap and recording the resulting voltages, $V_{i,r}^{VR+}$, for use in equation (4). The VRs are also adjusted down one tap to calculate the voltage sensitivity in that direction using equation (5). All voltages are calculated using full power flow solutions.

$$VSM_{i,j}^P = \frac{V_{i,j}^P - V_i^{Base}}{\Delta P} \quad \forall i \in N, \forall j \in N \quad (1)$$

$$VSM_{i,j}^Q = \frac{V_{i,j}^Q - V_i^{Base}}{\Delta Q} \quad \forall i \in N, \forall j \in N \quad (2)$$

$$VSM_{i,m}^{Cap} = V_{i,m}^{cap} - V_i^{Base} \quad \forall i \in N, \forall m \in M \quad (3)$$

$$VSM_{i,r}^{VR+} = V_{i,r}^{VR+} - V_i^{Base} \quad \forall i \in N, \forall r \in R \quad (4)$$

$$VSM_{i,r}^{VR-} = V_{i,r}^{VR-} - V_i^{Base} \quad \forall i \in N, \forall r \in R \quad (5)$$

B. Mixed-Integer Nonlinear Program

At each time step, a convex MINLP is solved to determine optimal dispatch for each controllable resource. The problem is solved using the BONMIN solver and GAMS modeling software. The objective of the MINLP is to minimize the cost of load control, PV curtailment, capacitor switching, and VR tap changes while reducing changes in voltage from one period to the next. The objective function contains a term for the cost of voltage deviation from the previous period which reflects benefits from limiting swings in voltages between time periods.

$$\min \sum_{i \in L} C_i^L + \sum_{k \in K} C_k^{PV} + \sum_{m \in M} C_m^{cap} + \sum_{r \in R} C_r^{VR} + \sum_{i \in N} \alpha_{\Delta V} \times [V_i^{t-1} - V_i(\cdot)]^2 \quad (6)$$

Subject to:

$$0 \le \Delta P_i^{L+} \le \overline{P_i^{L+}} \quad \forall i \in L \quad (7)$$

$$0 \le \Delta P_i^{L-} \le \overline{P_i^{L-}} \quad \forall i \in L \quad (8)$$

$$0 \le \Delta P_k^{PV} \le \overline{P_k^{PV}} \quad \forall k \in K \quad (9)$$

$$\frac{\left(\mathrm{Q^{Base}} + \sum_{k \in K} \Delta \mathrm{Q_k^{PV}} + \sum_{i \in L} (\Delta P_i^{L+} - \Delta P_i^{L-}) \times \frac{\sqrt{1 - pf_i^{L\,2}}}{pf_i^L} - \Delta Q^{Cap}\right)^2}{\left(\mathrm{P^{Base}} + \sum_{k \in K} \Delta \mathrm{P_k^{PV}} + \sum_{i \in L} (\Delta P_i^{L+} - \Delta P_i^{L-})\right)^2} \le \frac{1 - pf^2}{pf^2} \quad (10)$$

$$\left(\Delta Q_k^{PV}\right)^2 \le 1.1 \sqrt{(S_k^{PV})^2 - \left(\overline{P_k^{PV}} - \Delta P_k^{PV}\right)^2} \quad \forall k \in K \quad (11)$$

$$\underline{V} \le V_i(\cdot) \le \bar{V} \quad \forall i \in N \quad (12)$$

$$\Delta T_r^- + \Delta T_r^+ \le 1 \quad \forall r \in R \quad (13)$$

$$\Delta T_r^-, \Delta T_r^+, \Delta S_m \in \{0,1\} \quad \forall r \in R, m \in M \quad (14)$$

Note that

$$V_i(\cdot) = V_i^{Base} + \sum_{j \in N} VSM_{i,j}^P \times \left(\Delta P_j^{L+} - \Delta P_j^{L-} - \Delta P_j^{PV}\right) + \sum_{j \in N} VSM_{i,j}^Q \times \left(\Delta Q_j^{PV} + \frac{\sqrt{1 - pf_j^{L\,2}}}{pf_j^L} \times \left(\Delta P_j^{L+} - \Delta P_j^{L-}\right)\right) + \sum_{m \in M} VSM_{i,m}^{Cap} \times \Delta S_m + \sum_{r \in R} (\Delta T_r^+ \times VSM_r^{VR+} + \Delta T_r^- \times VSM_r^{VR-}) \quad (15)$$

and

$$\Delta Q^{Cap} = \sum_{m\in M'} \Delta S_m \times Q_m^{Cap} - \sum_{m\in M''} \Delta S_m \times Q_m^{Cap} \quad (16)$$

where $\overline{P_i^{L+}}$ and $\overline{P_i^{L-}}$ are the maximum controllable load increase and decrease at node i, respectively; $\overline{P_k^{PV}}$ is the maximum curtailable PV at node k; Q^{Base} and P^{Base} are the reactive and real power delivered to the circuit in the initial power flow before control; pf_i^L is the power factor of load at node i; pf is the desired power factor limit at the feeder head; S_k^{PV} is the rated capacity of PV at node k; $\underline{V}$ and $\overline{V}$ are the desired minimum and maximum voltage limits at all load nodes; $V_i(\cdot)$ is the estimated voltage at a node i after controls; and V_i^{t-1} is the voltage at node i from the previous time step's power flow solution. M' is the set of capacitors that are off and M'' is the set of capacitors that are on. Q_m^{Cap} is the kvar rating of capacitor m. The decision variables are $\mathbf{\Delta P^{L+}}$ and $\mathbf{\Delta P^{L-}}$, the vector of increase or decrease in load at all load nodes; $\mathbf{\Delta Q^{PV}}$, the vector of reactive power absorbed at all PV nodes; $\mathbf{\Delta P^{PV}}$, the vector of real power curtailment at all PV nodes; $\mathbf{\Delta S}$, the vector of the changes in all capacitor statuses; and $\mathbf{\Delta T^-}$ and $\mathbf{\Delta T^+}$, the vectors of negative or positive tap change at all VRs.

Equations (7-8) limit the real power increase and decrease at each controllable load to 20% of the unadjusted load at that node. Equation (9) limits the real power curtailment at each PV node to the current PV output at that node. Equation (10) constrains the power factor at the top of the feeder to limit excessive reactive power pushed to the transmission system. Equation (11) constrains the total real and reactive power from each PV system within its capacity. For this study, each inverter is sized such that its total apparent power can be up to 110% of its rated real power capacity, which increases the amount of reactive power that can be provided. Equation (12) limits voltage at all nodes to distribution ANSI limits. Equation (13) ensures that each VR cannot adjust up and down simultaneously in the model. Equation (14) restricts the tap change and capacitor switch variables to discrete values. Equation (15) uses the VSM to approximate the resulting voltage after control actions. Equation (16) gives ΔQ^{Cap}, the total change in reactive power injected by capacitors.

C. Resource Cost Functions

The cost functions of resources determine how the resources are dispatched in the MINLP. The formulations of the control cost functions are chosen to represent their price to the distribution operator and customer preferences.

1) Load Cost: In our feeder model, load nodes represent aggregated demand of multiple (5-10) customers. The diversity of loads allows for an assumption of continuous quantities of demand response (DR). In addition to modeling load reduction as a resource, this study assumes that the utility can motivate customers to increase load when needed. The model does not include any rebound effect representing load which is curtailed (or increased) in the current period being shifted to increased demand (or reduced demand) in the future. The cost curves of DR are represented as

$$C_i^L = \frac{\alpha_{Load}}{P_i^L} \times \left(\Delta P_i^{L+} + \Delta P_i^{L-}\right)^2 \quad \forall i \in L \quad (17)$$

Where P_i^L is the unadjusted load at node I and α_{Load} is a weighting factor for the cost of load deviations.

The quadratic cost function reflects increasing marginal costs with respect to quantity of DR acquired. The quadratic coefficient is dependent on the unadjusted load at the current time step to represent a higher marginal cost for loads with fewer customers (lower aggregated load) and at low load periods.

2) PV Cost: PV plant owners are assumed to accept prices for real power curtailment which are equal to the price for which they would have sold the power.

$$C_k^{PV} = \alpha_{PV} \times \Delta P_k^{PV} \quad \forall k \in K \quad (18)$$

Inverter-supplied reactive power is not costed directly. However, there is an opportunity cost for reactive power injection or absorption when it requires PV curtailment. Equation (11) models this relationship.

3) VR and Capacitor Cost: Unlike PV and load operation costs, capacitor and VR operational costs are influenced by the number of switching or tap changing events. Frequent operation of these devices can lead to increased maintenance and replacement costs. So, those devices have a constant price per operation.

$$C_m^{cap} = \alpha_{cap} \times \Delta S_m \quad \forall m \in M \quad (19)$$

$$C_r^{VR} = \alpha_{VR} \times \Delta T_r \quad \forall r \in R \quad (20)$$

Where α_{cap} and α_{LTC} are the costs of one capacitor switch or tap change, respectively.

The optimization parameters are listed in Table I.

TABLE I. OPTIMIZATION PARAMETERS USED IN CASE STUDY

Parameter	Value	Parameter	Value
$\boldsymbol{\alpha_{PV}}$	0.005	$\boldsymbol{\alpha_{cap}}$	0.1
$\boldsymbol{\alpha_{VR}}$	2	$\boldsymbol{pf}$	0.98
$\boldsymbol{\alpha_{Load}}$	0.1	$\boldsymbol{\Delta Q}$	5 kvar
$\boldsymbol{\alpha_{\Delta V}}$	0.5	$\boldsymbol{\Delta P}$	5 kW

III. SIMULATION SETUP

A real 3-phase unbalanced distribution feeder (see Fig. 1) in rural North Carolina is used to perform the case study. This feeder topology reflects typical distribution circuit expansions after progressive upgrades over years of load growth. Unlike IEEE test systems, the circuit has multiple long single-phase taps, making balancing load among phases difficult. Note that those phase imbalances often lead to single-phase control actions to keep voltages on all phases within limits. As shown in Fig. 1, the utility-owned assets include an LTC at the feeder head, one three-phase regulator, two single-phase regulators, and a three-phase 600 kvar capacitor bank. The LTC and voltage regulators are set to regulate at 125V with a bandwidth of ±1 V and a time delay between 30 and 90 seconds.

We use the hourly feeder-head load profile collected at the substation during a summer week in 2016 with the feeder load disaggregation algorithm presented in [11] to allocate 5-minute resolution load profiles to each load node. This step is crucial to give each load node a realistic individual load profile while ensuring that the aggregated load matches the measured feeder-head load profile.

To create the 20% PV penetration case, we add residential PV systems randomly to load nodes throughout the feeder until

the total PV capacity reaches 20% of the peak load. The PV system generation profiles are chosen from 147 residential PV profiles recorded by the Pecan Street project [12]. The power rating of each PV systems ranges from 3 kW to 10 kW. We assume that each PV system is equipped with a smart inverter that can inject and absorb reactive power. The resulting substation load, PV, and net load profiles are shown in Fig. 2. We also designed a 100% PV penetration case in the same way.

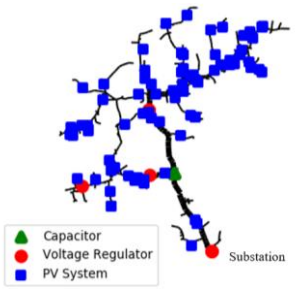

Fig. 1. Topology of a rural distribution feeder in North Carolina with 20% residential PV penetration.

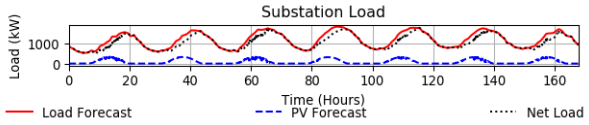

Fig. 2. Load, PV and net load for one summer week with 20% PV penetration.

In the base case, only utility-owned assets (i.e. LTC, VRs, and capacitor banks) are used to control voltage. The simulation runs for one week with 10-second time steps to capture the control actions of the voltage regulation devices with time delays under 5 minutes. Then, the results are down-sampled to 5-minute intervals to compare with the optimally controlled case.

In the optimally controlled case, the proposed algorithm is used to regulate voltage for the same week at a 5-minute control interval. In this case, loads, PV real and reactive power, regulators and capacitors were optimally dispatched based on the VSM-based MINLP algorithm.

IV. Simulation Results

A. Accuracy of the VSM-based Voltage Calculation

The accuracy of the voltage calculation using the VSM is crucial to the effectiveness of the voltage regulation as well as the computational speed of the algorithm. Figure 3 shows the difference between the estimated node voltages calculated during the optimization and the actual voltages calculated through power flow simulation after performing control operations prescribed by the optimization. The error is below 10^{-3} per unit, well within the error threshold for distribution operations. Compared with the previous VSM method used in [2], the accuracy is improved 10 times.

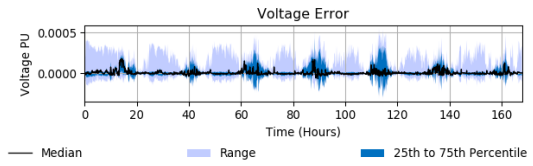

Fig. 3. Error between nodal voltages calculated using VSM and power flow.

B. Voltage Regulation

Figure 4 shows the distribution of the nodal voltage at each time step for the base case and with the VSM control method, both with 20% PV penetration. In the base case, the existing control scheme is not able to maintain all nodal voltages within the desired range. In the optimal control case, there are very few voltage violations. As shown in Fig. 5, a comparison between the histograms of the voltage violations shows that the VSM case reduces the magnitude of voltage violations in both cases, and reduces the frequency of violations significantly in the 20% PV case.

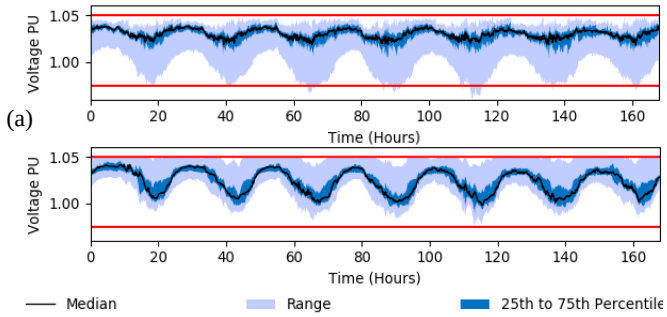

Fig. 4. Range, middle 50% and median node voltages at each time step for a) base case and b) proposed control method with 20% PV penetration.

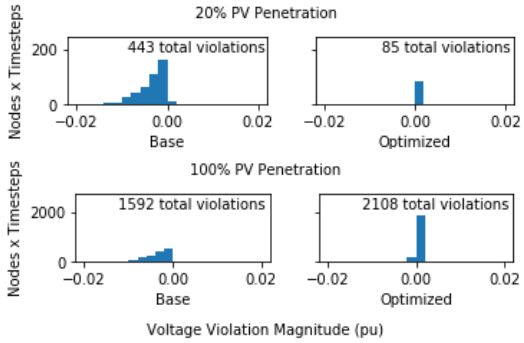

Figure 5. Number of nodes in violation of voltage limits, summed across all time steps.

In both the base case and the VSM case, the capacitor remains on for the entire week. In the base case, there are 341 tap changes or about 48 tap changes per day on average. In the VSM case (see Fig. 6), there were no regulator operations because all voltage control can be handled by PV and DR as dictated by the MINLP.

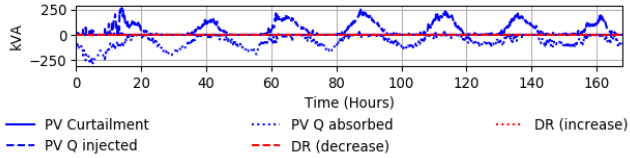

Fig. 6. Optimal control actions for one week with 20% PV penetration.

Table II compares the total amount and cost of all control actions for each case. Note that the operational cost of the base case control increases as more PV is added, but that in the optimally controlled case, the higher PV penetration allows for cheaper control thanks to an abundance of free reactive power.

Since this method uses significant reactive power injection and absorption to regulate voltages, power factor can become a concern. In Fig. 7, we can see that by including a constraint on power factor at the top of the feeder within the MINLP, the

power factor is successfully maintained between .98 leading and .98 lagging throughout the simulated week despite heavy use of reactive power.

TABLE II. OVERALL NUMBER OR QUANTITY OF EACH CONTROL ACTION AND THEIR COSTS FOR THE BASE CASE AND OPTIMAL CASE.

20% PV Penetration Case				
	Existing Control		VSM Control	
	Actions	Costs	Actions	Costs
Capacitor Switches	0	$ 0	0	$ 0
Tap Changes	341	$ 170.50	0	$ 0
PV Curtailment (kWh)	-	-	27	$ 1.64
Inverter Q Injection (kvarh)	-	-	9,169	-
Inverter Q Absorption (kvarh)	-	-	10,680	-
Demand Response (kWh)	-	-	4	$ 0.33
Total Cost		$ 170.50		$ 1.97
100% PV Penetration Case				
	Existing Control		VSM Control	
	Actions	Costs	Actions	Costs
Capacitor Switches	0	$0	0	$ 0
Tap Changes	433	$216.50	0	$ 0
PV Curtailment (kWh)	-	-	10	$ 0.57
Inverter Q Injection (kvarh)	-	-	16,223	-
Inverter Q Absorption (kvarh)	-	-	11,409	-
Demand Response (kWh)	-	-	15	$ 0.05
Total Cost		$216.50		$ 0.62

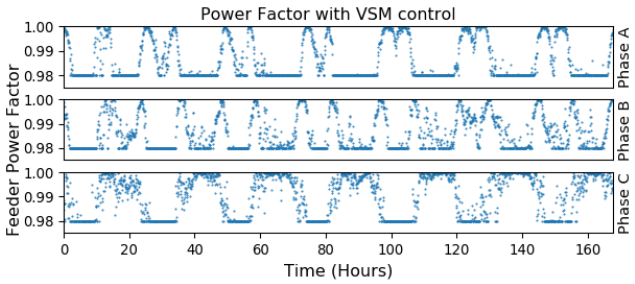

Fig. 7. Power factor at the substation with optimal control.

C. Computational Speed

Finally, we consider the computational time necessary to calculate the VSM and optimize resource dispatch. This metric determines whether it is possible to run this algorithm in real time as an operational tool. Fig. 8 shows a boxplot of the computational time to calculate the VSM and solve the MINLP for each time step. All time steps are completed well within the 5-minute requirement and the majority of scenarios run in under one minute on a computer with an intel i7-4770 processor. Other volt-var control algorithms are often tested on smaller circuits and with fewer decision variables. However, we can make a rough comparison to the algorithm in [6] which is tested on a circuit of similar size using no DR and only 5 DERs (compared to 85 PVs in our test case). Our VSM and MINLP solution takes an average 13.5 seconds compared to 1.51 seconds for their discrete coordinate descent algorithm.

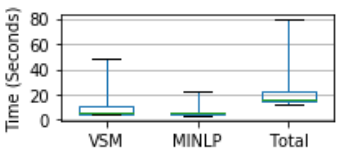

Fig. 8. Boxplots showing the median (line), 25th and 75th percentiles (box) and range (whiskers) for time to calculate the VSM, time to solve the MINLP, and the total run time for each time step for the 20% PV case.

V. DISCUSSION

The case study demonstrates that the proposed method can improve voltage control while minimizing operational costs. This method can be adapted for various distribution system operators based on their specific costs and operational goals. For example, this method could be used to deploy conservation voltage reduction by lowering the desired maximum voltage constraint in the MINLP. Likewise, utilities with different operational costs for PV curtailment, load participation, and utility-owned device operations can adjust the cost parameters to match their situation. Therefore, this method is highly versatile and could be employed by any DSO that has some or all of the devices mentioned. The main limitation of this method is the need for extensive communication infrastructure and buy-in from consumers and PV producers. These challenges could be mitigated through targeted recruitment of large customers and PV operators who can have significant control impacts with only a few communication links. Future work will include investigation into how factors like PV size and location affect the voltage control capability and costs. That work will help determine the most effective ways to recruit for participation in the control scheme which would reduce the capital and operational costs associated with this method.

VI. REFERENCES

[1] W. Ren and H. Ghassempouraghamolki, "Tuning of Voltage Regulator Control in Distribution," in *IEEE Power and Energy Society General Meeting*, Portland, 2018.

[2] X. Zhu, J. Wang, D. Mulcahy, D. L. Lubkeman, N. Lu, N. Samaan and R. Huang, "Voltage-Load Sensitivity Matrix Based Demand Response for voltage Control in High solar Penetration Distribution Feeder," in *IEEE Power & Energy Society General Meeting*, Chicago, 2017.

[3] Q. Zhou and J. W. Bialek, "Simplified Calculation of Voltage and Loss Sensitivity Factors in Distribution Networks," in *16th Power Systems Computation Conference (PSCC 2008)*, Glasgow, Scotland, 2008.

[4] K. Christakou, J.-Y. LeBoudec, M. Paolone and D.-C. Tomozei, "Efficient computation of Sensitivity Coefficients of Node Voltages and Line Currents in Unbalanced Radial Electrical Distribution Networks," *IEEE Transactions on Smart Grid*, vol. 4, no. 2, pp. 741-750, 2013.

[5] K. Christakou, D.-C. Tomozei, J.-Y. Le Boudec and M. Paolone, "GECN: Primary Voltage Control for Active Distribution Networks via Real-time Demand-Response," *IEEE Transactions on Smart Grid*, vol. 5, no. 2, pp. 662-631, 2014.

[6] R. A. Jabr and I. Džafić, "Sensitivity-Based Discrete Coordinate-Descent for Volt/VAr Control in Distribution Networks," *IEEE Transactions on Power Systems*, vol. 31, no. 6, pp. 4670 - 4678, 2016.

[7] Z. Zhang, L. F. Ochoa and G. Valverde, "A novel Voltage Sensitivity Approach for the Decentralized Control of DG Plants," *IEEE Transactions on Power Systems*, vol. 33, no. 2, pp. 1566-1576, 2018.

[8] S. Conti, S. Raiti and G. Vagliasindi, "Voltage sensitivity analysis in radial MV distribution networks using constant current models," in *IEEE International Symposium on Industrial Electronics*, Bari, Italy, 2010.

[9] M. Kraiczy, B. York, M. Bello, D. Montenegro, S. Akagi and M. Braun, "Coordinating Smart Inverters with Advanced Distribution Voltage Control Strategies," in *IEEE Power and Energy Society General Meeting*, Portland, 2018.

[10] A. Singhal and V. Ajjarapu, "A Framework to Utilize DERs' VAR Resources to Support the Grid in an Integrated T-D System," in *IEEE Power and Energy Society General Meeting*, Portland, 2018.

[11] J. Wang, et al. "A Two-Step Load Disaggregation Algorithm for Quasi-static Time-series Analysis on Actual Distribution Feeders," in *IEEE Power and Energy Society General Meeting*, Portland, 2018.

[12] Residential load data collected by PECAN STREET website: https://dataport.pecanstreet.org/data/interactive